^{15}N NMR Relaxation Studies of Free and Inhibitor-Bound 4-Oxalocrotonate Tautomerase: Backbone Dynamics and Entropy Changes of an Enzyme upon Inhibitor Binding†

James T. Stivers, Chitrananda Abeygunawardana, and Albert S. Mildvan*

Department of Biological Chemistry, The Johns Hopkins School of Medicine, 725 North Wolfe Street, Baltimore, Maryland 21205-2185

Christian P. Whitman

Medicinal Chemistry Division, College of Pharmacy, The University of Texas, Austin, Texas 78712-1074

Received July 24, 1996; Revised Manuscript Received October 18, 1996⊗

ABSTRACT: The solution secondary structure of 4-oxalocrotonate tautomerase (4-OT), a 41 kDa homohexamer with 62 residues per subunit, consists of an α-helix, two β-strands, a β-hairpin, two loops, two turns, and a C-terminal coil [Stivers et al. (1996) *Protein Sci. 5*, 729−741]. The general base, proline-1, as well as the two loops and the β-hairpin have been shown to comprise the active site [Stivers et al. (1996) *Biochemistry 35*, 814−823]. The backbone dynamics of both the free enzyme and its complex with a substrate analog have been studied by ^{1}H-detected ^{15}N relaxation rates and NOE determinations at 500 and 600 MHz. Analysis of the data using the model-free formalism showed that the nanosecond to picosecond motion of 53 of the 60 backbone ^{15}N−H vectors was highly restricted with a mean order parameter $\langle S^2 \rangle = 0.87 \pm 0.03$. The lowest backbone mobility ($S^2 > 0.90$) is found in the β1-strand, loop 2, and turn 2. Greater backbone mobility is found in the active site ($0.5 \leq S^2 \leq 0.83$) and at C-terminal residues 58−62 ($0.03 \leq S^2 \leq 0.70$). A τ_m value for the free hexamer of 13.7 ns at 42 °C was determined, consistent with a compact globular molecule of 41 kDa. Saturation of 4-OT with the analog of the dienolic intermediate and linear competitive inhibitor *cis,cis*-muconate (**4**) ($K_D = 0.59$ mM) *increased* the backbone S^2 of seven residues and *decreased* the backbone S^2 of another eight residues, both at the active site and at the antiparallel β1−β1 interface. The S^2 values of the other 44 detectable NH vectors were not altered by the binding of **4**. The increases in S^2, resulting from the "freezing" of the backbone NH vectors of seven residues upon the binding of **4**, correspond to an unfavorable entropic contribution to $\Delta G_{binding}$ of 3.2 ± 1.1 kcal/mol. This freezing is partially compensated for by the mobilization of the other eight residues, since the decreases in S^2 for these residues correspond to an entropic contribution to binding of −1.9 ± 0.1 kcal/mol. These entropy changes, resulting solely from alterations in high-frequency motion, are significant compared to the overall $\Delta G_{binding} = -4.6$ kcal/mol for **4**. Other effects of the binding of **4** include (1) changes in ^{15}N and NH chemical shifts localized to the active site and (2) increases in the exchange contributions (R_{ex}) to $1/T_2$ of backbone ^{15}N resonances at the active site and at the subunit interface, reflecting microsecond to millisecond motions which may play a role in substrate binding ($k_{on} \geq 4 \times 10^6$ M^{-1} s^{-1}) and/or catalysis ($k_{cat} = 10^3$ s^{-1}).

The role of internal motions of proteins both in catalysis and in specific ligand binding is a subject of great interest which has been stimulated by theoretical advances (Lipari & Szabo, 1982a,b; Clore et al., 1990a,b; Palmer et al., 1991), by the development of isotopic labeling methods, and by heteronuclear NMR techniques for measurement of relaxation rates of individual nuclei in proteins (Peng & Wagner, 1994, and references therein). Despite these methodological advances, no unified picture has yet emerged as to the functional role of fast or slow time scale protein motions in binding specificity or catalysis.

The restriction of conformational freedom in enzyme−substrate complexes is frequently proposed to contribute to enzymatic catalysis. It has been suggested that residues in active sites are mobile in the uncomplexed state and that their motions, like those of the bound substrate, become more highly restricted in the complex in order to constrain the substrate to a conformation that resembles the transition state [reviewed in Mildvan (1974)]. A recent example is provided by the catalytic tyrosine residue of Δ^5-3-ketosteroid isomerase which, upon steroid binding, shows a decrease in amplitude of the high-frequency motion of its phenolic side chain but no significant change in the motion of its backbone C_α (Zhao et al., 1996). However, there is an entropic penalty for the immobilization of a residue upon substrate or ligand binding, and this unfavorable entropy change must be offset by the intrinsic binding energy of the ligand for the protein (Jencks, 1987). Therefore, if an enzyme or protein can minimize the entropic penalties associated with complex formation, more of the intrinsic binding energy is available for transition state stabilization or higher affinity binding.

† This work was supported in part by National Institutes of Health Grants DK28616 (to A.S.M.) and GM41239 (to C.P.W.). J.T.S. is an American Cancer Society Postdoctoral Fellow.

* Address correspondence to this author: phone, 410-955-2038; FAX, 410-955-5759.

⊗ Abstract published in *Advance ACS Abstracts,* December 1, 1996.

S0006-2960(96)01834-X CCC: $12.00

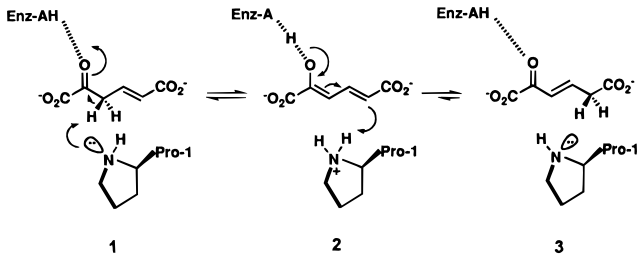

FIGURE 1: Minimal catalytic mechanism of 4-oxalocrotonate tautomerase (Stivers et al., 1996a,b). Proline-1 ($pK_a = 6.4$), the general base, removes the 3-proton of substrate **1**, concerted with electrophilic catalysis at the C-2 oxygen atom by a putative enzymic general acid ($pK_a = 9.0$). For simplicity, the enolization is shown as concerted. The dienolic intermediate **2** is then reketonized and protonated stereospecifically at the 5-position to yield the *pro-S* enantiomer of **3** (Whitman et al., 1992).

The backbone and side chain dynamics of several free and ligand-bound proteins including enzymes have been studied using ^{13}C (Nicholson et al., 1992; Zhao et al., 1996), ^{15}N (Akke et al., 1993; Cheng et al., 1994; Rischel et al., 1994; Farrow et al., 1994; Epstein et al., 1995; Mandel et al., 1995), and ^{2}H-based (Kay et al., 1996) NMR spin relaxation experiments. The results of many of these studies have provided evidence in support of the proposal that ligand binding induces a localized restriction of side chain and backbone motion near the ligand binding site. However, in a detailed study of the effects of phosphotyrosine-peptide binding on the dynamics of the Src homology 2 domain (SH2), more complicated observations were made. In the backbone, there was no simple relationship between peptide binding and changes in picosecond time scale motions at the peptide binding site (Farrow et al., 1994). With respect to the side chains, some groups involved in peptide binding were immobilized by complex formation, while others were mobile in both the presence and absence of peptide. The mobile residues were suggested to be important for minimization of the entropic penalty associated with complex formation (Kay et al., 1996). A similar detailed comparison of the dynamics of a free and complexed enzyme has not previously been reported.

4-Oxalocrotonate tautomerase (4-OT,[1] EC 5.3.2) is a homohexameric enzyme (MW = 41 000, 62 residues/subunit) that catalyzes the isomerization of unconjugated α-keto acids, such as **1**, to the conjugated isomer **3** via a dienolic intermediate, **2** (Figure 1). The small subunit size of 4-OT makes it an attractive model for studying the mechanism and structure of a keto−enol tautomerase in solution using heteronuclear NMR spectroscopy. Recent NMR and mechanistic studies of 4-OT have established (1) the backbone and side chain ^{1}H, ^{15}N, and ^{13}C NMR assignments and the solution secondary structure of the free enzyme (Stivers et al., 1996c), (2) that the enzyme has six active sites per hexamer, and (3) that the amino-terminal proline residue ($pK_a = 6.4$) is the catalytic base (Stivers et al., 1996a,b). A 1.9 Å resolution crystal structure of a highly homologous isozyme of 4-OT (Subramanya et al., 1996) agrees well with the NMR structure of 4-OT and shows that the enzyme consists of a trimer of dimers (Figure 2A). Active site regions of the enzyme have been localized to Pro-1, loops 1 and 2, and the β-hairpin (Stivers et al., 1996a−c).

In this work we report the complete backbone ^{15}N dynamics of free 4-OT and its complex with the competitive inhibitor *cis*,*cis*-muconate (**4**), which resembles the dienolic

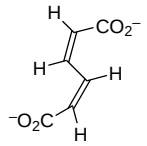

4

intermediate **2** (Figure 1), using $^{1}H-^{15}N$ NMR relaxation measurements. To our knowledge, this represents the first report of the backbone dynamics of a free and complexed enzyme. A preliminary report of this work has been published (Abeygunawardana et al., 1996), and a forthcoming paper will treat the side chain dynamics of free 4-OT and its complex with **4**.

EXPERIMENTAL PROCEDURES

Materials and General Methods. 2-Hydroxymuconate (**2**) for isomerase assays was synthesized as previously described (Whitman et al., 1991). Catechol (99+%) and peracetic acid (32 wt %) were from Aldrich. $^{2}H_2O$ (99.996 atom %) and $^{15}NH_4Cl$ (99 atom %) were obtained from Cambridge Isotope Labs (Woburn, MA). Uniformly ^{15}N-labeled 4-OT was obtained as described previously using the T7-based expression system (Stivers et al., 1996a). All other solvents and reagents were of the highest quality commercially available. All buffers used in the NMR experiments were deionized with Chelex-100 resin and filtered through a 0.22 μm filter (Millipore) before addition to the NMR samples.

Synthesis of 4. **4** was prepared by the Fe(III)-catalyzed oxidation of catechol with peracetic acid (Pandell, 1976). To a 50 mL Erlenmeyer flask containing a magnetic stir bar was added 5.0 mL of glacial acetic acid, 15 mL of 32% peracetic acid (5.52 g, 0.0726 mol), and then 0.140 mL (3.2 mg, 0.168 mmol) of a $FeCl_3$ solution which had been freshly prepared by dissolving 48 mg of the ferric salt in 2.13 mL of glacial acetic acid. To this solution, over a period of 5 h at room temperature, was added a 10 mL solution of catechol prepared by dissolving 3.07 g (0.0279 mol) of catechol in glacial acetic acid. After the addition was complete, the reaction was cooled at 4 °C for 20 min and then filtered with suction using a medium frit glass filter. The precipitate was washed with 20 mL of glacial acetic acid, followed by 5 mL washings with ice-cold deionized water (50 mL total). The product was dried in an evacuated desiccator *vs* P_2O_5 and KOH for 14 h at room temperature. The final yield was 1.5 g (38%) of the free acid: ^{1}H NMR (acetone-d_6, 600 MHz) δ 6.03 (dd, 2H), 7.89 (dd, 2H). From the NMR spectrum, the purity of **4** was >98%.

Preparation of NMR Samples. The NMR sample of the free enzyme contained 2.4 mM 4-OT subunits in 0.62 mL of $H_2O/^{2}H_2O$ (90:10) and 26 mM potassium phosphate buffer at pH 6.45. The NMR sample of the 4-OT complex with **4** was obtained from the final titration sample described below. The final concentration was 3.2 mM in 4-OT subunits and

[1] Abbreviations: 4-OT, 4-oxalocrotonate tautomerase; **1**, 2-oxo-4-hexenedioate; **2**, 2-hydroxy-2,4-hexadienedioate; **3**, 2-oxo-3-hexenedioate; **4**, 2,4-hexadienedioate (CCM, *cis*,*cis*-muconate); FID, free induction decay; R_1, longitudinal relaxation rate; R_2, transverse relaxation rate; CSA, chemical shift anisotropy; TSP, 3-(trimethylsilyl)-propionate-*2,2,3,3-d*$_4$.

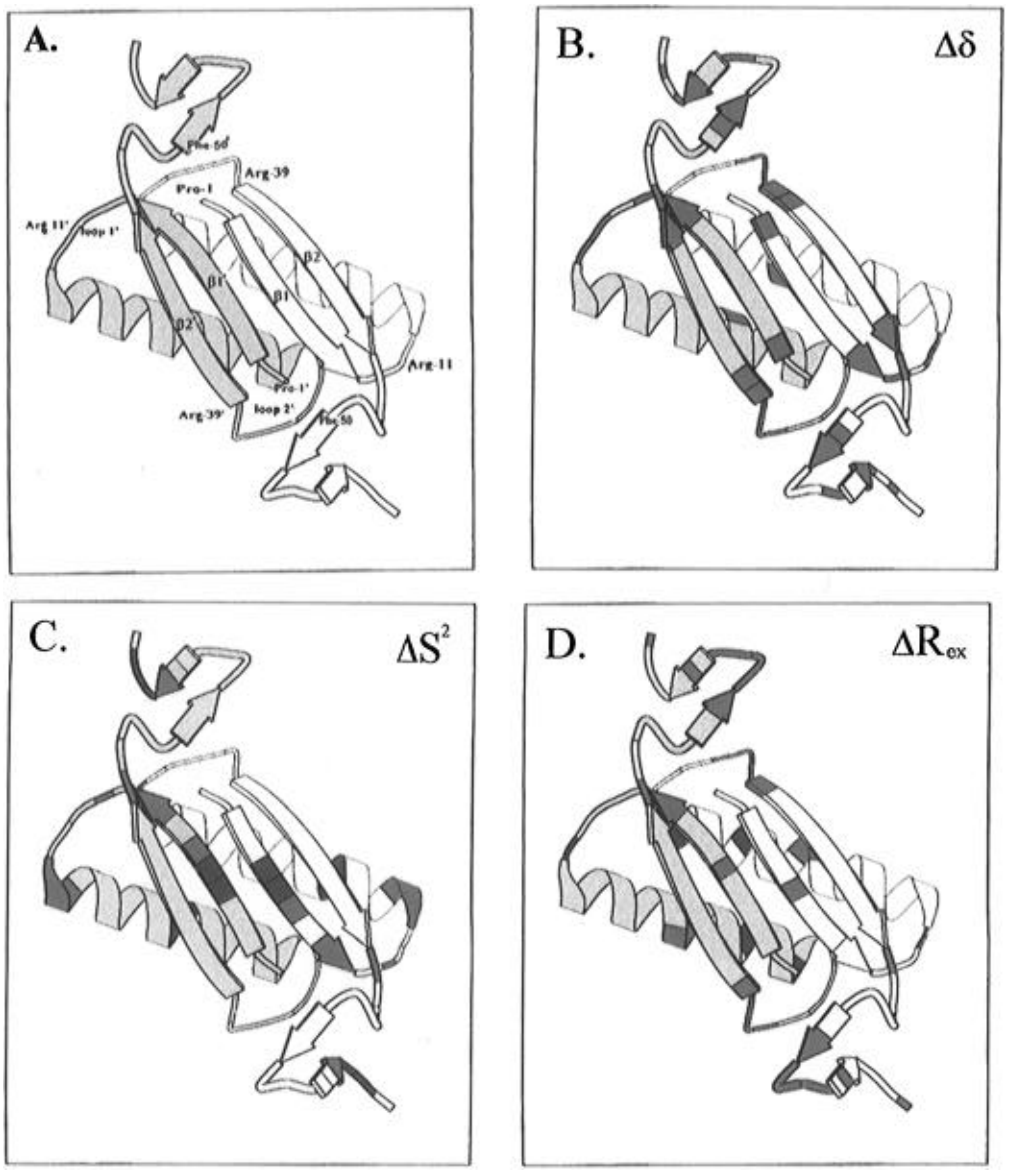

FIGURE 2: Tertiary structure of the 4-OT dimer unit and the changes in backbone amide chemical shifts ($\Delta\delta$), order parameters (ΔS^2), and exchange contributions (ΔR_{ex}) to ^{15}N transverse relaxation upon binding of **4**. (A) Tertiary structure of 4-OT as seen in the 1.9 Å crystal structure of Subramanya et al. (1996). Major active site residues are indicated, and primed residues are in the adjacent subunit. (B) Changes in amide nitrogen and proton chemical shifts of 4-OT upon binding of **4**. Residues that showed combined chemical shift changes greater than the threshold line shown in Figure 4C are marked in red. (C) Changes in backbone order parameters upon binding of **4**. Residues that showed a significant increase in mobility upon binding of **4** are marked in red, and those that showed a decrease in mobility are marked in blue. (D) Changes in the exchange contribution to the ^{15}N line width upon binding of **4**. Residues that showed a significant increase in R_{ex} upon binding of **4** are marked in red, and those that showed a decrease in R_{ex} are marked in blue.

20.5 mM **4** in $H_2O/^2H_2O$ (90:10) at pH 6.45. Using a pK_a of 6.5 for the phosphate dianion and the free **4** dianion concentration of 17.3 mM, an ionic strength of 52 mM is calculated for both the free and complexed 4-OT NMR samples. All NMR determinations were carried out at 42.0 °C, and the free enzyme retained more than 85% of its initial activity after 2 weeks at this temperature.

*Determination of K_D for Binding of **4**.* Since the 4-OT−**4** complex is in fast exchange on the chemical shift time scale (see Results), and the amide ^{15}N and ^1H assignments of the free enzyme have already been made (Stivers et al., 1996c), the dissociation constant (K_D) and the amide ^{15}N and ^1H assignments for the complex were determined by titration of the enzyme with **4**, following the changes in the amide ^1H and ^{15}N chemical shifts in a series of $^1H-^{15}N$ HSQC spectra at 600 MHz. The water flip-back pulse sequence of Mori et al. (1995) was used, employing sweep widths of 8000 and 1884 Hz in the proton and ^{15}N dimensions, respectively. Using States−TPPI, a total of 256 t_1 values with two or four scans per FID were acquired. The final matrix sizes, after zero filling were 1K × 1K real points. For these titrations, a ~100 mM aqueous stock solution of **4** was prepared gravimetrically and adjusted to pH 6.45 with 1 M Tris base. This solution was deionized by passage through a small column containing Chelex-100 resin, and the final exact concentration was determined by absorbance at 257 nm (ϵ = 15 900 M^{-1} cm^{-1}, dianion, water). The titration was performed by adding small portions (2−45 μL) of a stock solution of **4** to a solution of 4-OT (620 μL, $[4\text{-OT}]_0$ = 4.0 mM in subunits). The absolute values of the chemical shift changes ($\Delta\delta_{obs} = |\delta - \delta_0|$) for three well-resolved resonances with the largest $\Delta\delta_{max}$ values (R11, R39, G51) were plotted against the total concentration of **4** (L_{tot}) and used to determine K_D according to eq 1, where E_{tot} is

$$\Delta\delta_{obs} = \left[\frac{\Delta\delta_{max}}{2E_{tot}}\right]\{K_D + E_{tot} + L_{tot} - [(K_D + E_{tot} + L_{tot})^2 - 4E_{tot}L_{tot}]^{1/2}\} \quad (1)$$

$$E_{tot} = \frac{[4\text{-OT}]_0}{(1 + d_f L_{tot})}$$

the normalized enzyme concentration at each titration point taking into account dilution effects (d_f = dilution factor/L_{tot}).

Inhibition Kinetics. To determine whether **4** was a competitive inhibitor of the isomerization of **2**, a kinetic analysis was performed. Since **4** has a strong UV absorption band at 236 nm, the wavelength at which the rate of formation of **3** is usually monitored (Whitman et al., 1991), it was necessary to monitor the disappearance of **2** at 310 nm (ϵ = 19 416 M^{-1} cm^{-1}) where the absorption of **4** is less significant. Using this method, the inhibition by increasing concentrations of **4** (0, 0.456, 0.912, and 3.64 mM) was studied at five concentrations of **2** in the range 0.028−0.228 mM. After correcting for background rates at each substrate concentration, the data were analyzed using double-reciprocal plots of $1/v$ against 1/[S] at each concentration of **4**. The K_I for **4** was then determined from the slope of a plot of K_m^{app} against [**4**].

NMR Spectroscopy. All NMR experiments were performed on Varian Unity^{plus} 500 and 600 NMR spectometers equipped with *z* gradient capabilities, using Varian 5 mm triple resonance, pulsed field gradient probes. The temperature calibrations (42 °C) in different spectrometers were obtained by adjusting the set temperature to produce a chemical shift difference of 4.61 ppm between the proton signal of HOD and TSP in a standard sample of TSP dissolved in ^2H_2O. The ^1H chemical shifts are reported with respect to the H_2O signal, which is 4.61 ppm downfield from external TSP at 42 °C. The nitrogen chemical shifts are reported with respect to external $^{15}NH_4Cl$ (2.9 mM in 1 M HCl) at 20 °C, which is 24.93 ppm downfield from liquid NH_3 (Levy & Lichter, 1979).

The ^{15}N relaxation data were obtained using the water flip-back, sensitivity-enhanced pulse sequences of Farrow et al. (1994), which employ pulsed field gradients to select for the coherence transfer pathway, to minimize spectral artifacts, and to suppress the solvent resonance. All experiments utilized a total of 1024 and 256 complex points in F_2 (^1H) and F_1 (^{15}N), respectively. For the R_1 and R_2 experiments, 8 scans were collected per t_1 point, and for the $^1H-^{15}N$ NOE experiments, 16 scans per t_1 point were acquired. The ^1H and ^{15}N carriers were positioned at 4.61 and 118.5 ppm, respectively. All experiments used a proton sweep width of 8000 Hz and ^{15}N sweep widths of 1600 and 1884 Hz for the experiments at 500 and 600 MHz, respectively.

The ^{15}N R_1 and R_2 values at 600 MHz were obtained using 10 delays (*T*): 0.20, 0.40, 0.60, 0.80, 1.00, 1.20, 1.40, 1.60, 1.80, and 2.00 s for the R_1 experiment and 0.017, 0.034, 0.051, 0.068, 0.085, 0.101, 0.118, 0.135, 0.152, and 0.169 s for the R_2 experiment. The ^{15}N R_1 and R_2 values at 500 MHz were obtained using 8 delays: 0.24, 0.49, 0.73, 0.98, 1.22, 1.47, 1.71, and 1.95 s for the R_1 experiment and 0.017, 0.033, 0.050, 0.066, 0.083, 0.099, 0.116, and 0.132 s for the R_2 experiment. Data for each relaxation experiment were acquired in an interleaved manner in which alternate FIDs were collected for each relaxation delay (*T*) before chemical shift labeling in the ^{15}N dimension. The recycle time was 2.6 s for the ^{15}N R_1 and R_2 experiments. While this was only ~1.6-times the T_1 of the average NH proton, such rapid data collection with the pulse sequence used has been shown to decrease only the sensitivity of the ^{15}N relaxation measurements without introducing systematic errors (Sklenar et al., 1987).

The $^1H-^{15}N$ steady-state NOE values at 500 and 600 MHz were obtained by recording spectra with and without a proton presaturation period (4.0 s) applied before the start of the $^1H-^{15}N$ HSQC experiment and a recycle time of 10 s. Control experiments demonstrated that the NOE reached steady state with presaturation periods of 3 s or longer. The NOE spectra were acquired in an interleaved manner, in which each individual FID was collected with and without proton presaturation.

Data Processing and Analysis. All spectra were processed identically on a Silicon Graphics Personal IRIS 4D/35 workstation using the FELIX software package (Biosym Technologies, Inc.). The acquired time domain t_1 data points were extended by one-third of their original size by the forward linear prediction routine in FELIX. A 60° sine bell and a 90° sine squared bell filter were applied in the first and second dimensions, respectively. To increase the signal-to-noise ratio, the NOE experiments at 500 and 600 MHz for free 4-OT were also processed using exponential multiplication (line broadening = 20 Hz). The final matrix sizes were 1024 × 1024 real points after zero filling.

The peak heights in the 2D spectra were measured using the peak-picking subroutine in FELIX. The R_1 and R_2 values were determined by fitting the peak heights as a function of relaxation interval (*t*) to a two-parameter (I_0 and $R_{1,2}$) or three-parameter (I_0, I_∞, and $R_{1,2}$) exponential decay (eq 2 and 3,

$$I(t) = I_0 \exp(-R_{1,2}t) \quad (2)$$

$$I(t) = I_\infty - (I_\infty - I_0) \exp(-R_{1,2}t) \quad (3)$$

respectively) using a nonlinear least-squares analysis (Leatherbarrow, 1992). Only 4 of the 60 detectable backbone ^{15}NH resonances (Q4, I5, H6, L35) were significantly improved by using the three-parameter equation as judged by an *F* statistical analysis (Stone et al., 1992, 1993). The I_∞ values for these residues were within the noise levels of the spectra and thus indistinguishable from zero. The uncertainties in the $R_{1,2}$ values were taken as the standard errors of the fits, assuming that the standard deviation in the data points is approximated by the standard deviation of the points from the fitted curve (Press et al., 1992).

The steady-state NOE values at 500 and 600 MHz were determined from the ratios of the peak intensities with and without proton presaturation (eq 4). The standard deviation

$$\text{NOE} = I_{sat}/I_{eq} \quad (4)$$

of the NOE was determined from the root-mean-square value of the background noise in the spectra as described (Farrow et al., 1994).

Relaxation Theory. The theory of $^{15}N-^1H$ NMR relaxation has been discussed in detail elsewhere (Peng & Wagner, 1994; Clore et al., 1990a,b; Palmer et al., 1991), and therefore, only a brief discussion is presented here. The

NMR relaxation parameters R_1, R_2, and NOE are functions of the spectral density function, $J(\omega)$, which in turn depends on the overall correlation time (τ_m) for molecular tumbling as well as the amplitudes and rates of any internal motions which may be occurring. The measurement of three NMR relaxation parameters, even at two frequencies as was done here, is insufficient to characterize these motions in detail. Therefore, an approximation of $J(\omega)$ is needed, which is provided by the so-called "model-free" formalism of Lipari and Szabo (1982a,b). The model-free approach characterizes the internal motions of a given $^{15}N-^{1}H$ vector in terms of a generalized order parameter, S^2, and an internal correlation time, τ_e. S^2 is a measure of the degree of spatial restriction of the N−H vector relative to the fixed molecular frame of reference, and its value ranges from 0, for unrestricted internal motion, to 1, for complete restriction of internal motion. The internal correlation time, τ_e, is an indicator of the rate of these motions. The Lipari and Szabo approximation of the spectral density is expressed as

$$J(\omega) = (2/5)\left(\frac{S^2\tau_m}{1+\omega^2\tau_m^2} + (1-S^2)\frac{\tau}{1+\omega^2\tau^2}\right) \quad (5)$$

where $\tau = \tau_m\tau_e/(\tau_m + \tau_e)$, S^2 and τ_e are optimized for each residue, and τ_m is fixed for the whole molecule. When $\tau_e \ll \tau_m$, and when S^2 approaches 1, eq 5 simplifies to

$$J(\omega) = (2/5)\left(\frac{S^2\tau_m}{1+\omega^2\tau_m^2}\right) \quad (5A)$$

The model-free analysis may also be extended to approximate internal motions on two time scales (Clore et al., 1990a,b). The corresponding spectral density function is now expressed as a function of three motions (eq 6), τ_m, a time constant for overall rotational tumbling, and two time constants (τ_e and τ_f) with their corresponding order parameters ($S_s^2$and S_f^2) to describe internal motions faster than τ_m. For such a system, $S^2 = S_f^2S_s^2$. In eq 6 (where τ is defined

$$J(\omega) = (2/5)\left(\frac{(S_f^2S_s^2)\tau_m}{1+(\omega\tau_m)^2} + \frac{S_f^2(1-S_s^2)\tau}{1+(\omega\tau)^2} + \frac{(1-S_f^2)\tau_1}{1+(\omega\tau_1)^2}\right) \quad (6)$$

$$\tau_1 = \frac{\tau_f\tau_m}{\tau_f+\tau_m}$$

above), the relative contribution to $J(\omega)$ of the middle term containing τ_e is given by the order parameter S_s^2, and the relative contribution to $J(\omega)$ of the last term containing τ_f is given by S_f^2. The last term in eq 6 containing τ_f was not needed to fit the data because, when $\tau_1 \sim \tau_f < 10$ ps, this term does not contribute to the ^{15}N relaxation process.

To obtain satisfactory back-calculations of R_2 (eq 7), it is sometimes necessary to incorporate an exchange contribution (R_{ex}) to transverse relaxation, in addition to the dipole−dipole terms for fast internal motions ($R_{2(DD)}$) and the chemical shift anisotropy contribution ($R_{2(CSA)}$). Such exchange contributions to R_2 result from conformational exchange occurring on the microsecond to millisecond time scale.

$$R_2 = R_{2(DD)} + R_{2(CSA)} + R_{ex} \quad (7)$$

Simulations Using the Model-Free Formalism. Model-free parameters were determined from R_1, R_2, and $^1H-^{15}N$ NOE measurements at 500 and 600 MHz (^1H frequencies) using the program Modelfree 3.1 (Palmer et al., 1991). The spin relaxation of the ^{15}N nucleus is dominated by the dipolar coupling with the attached proton and the chemical shift anisotropy (CSA) of the ^{15}N nucleus (Abragam, 1961). Therefore, an internuclear N−H distance of 1.02 Å was used in the simulations of the NOE measurements, and an axially symmetric chemical shift tensor for ^{15}N was assumed with $(\sigma_{||} - \sigma_{\perp}) = -160$ ppm (Hiyama et al., 1988). Calculation of the model-free parameters from the data was performed by optimizing a target function [χ^2; see Palmer et al. (1991)] which minimizes the differences between the experimental and calculated R_1, R_2, and NOE values relative to the experimental error associated with each measurement. Uncertainties in each of the parameters were taken to be the standard deviations of the distributions around the mean values derived from 500 Monte Carlo simulations (Palmer et al., 1991).

To determine the correct spectral density function, it is first necessary to estimate a value for the overall correlation time, τ_m. As previously described, the R_2/R_1 ratio may be used to estimate τ_m provided that τ_e and chemical exchange terms are not significant (Kay et al., 1989; Clore et al., 1990a). Therefore, residues with a R_2/R_1 ratio greater than or less than one standard deviation from the mean value for all residues should be excluded when calculating this initial estimate. Using this method, an initial value for $\tau_m = 14.2 \pm 0.4$ ns for free 4-OT was obtained using a trimmed weighted mean R_2/R_1 ratio of 14.74 and 19.52 at 500 and 600 MHz, respectively.

The appropriate spectral density function for each residue was selected by initially fitting the data to the simplest spectral model (eq 5) and resorting to more complicated models (*i.e.*, eq 6, and/or including R_{ex}) only when required to fit the relaxation data [see Farrow et al. (1994)]. The experimental data at 500 and 600 MHz were fit simultaneously and were considered to be adequately modeled if the R_1 and R_2 data were reproduced to within 5% and the NOE data to within ±10% of their experimentally determined values.

RESULTS

*$^1H-^{15}N$ Chemical Shift Assignments and K_D for the Complex of **4** with 4-OT.* Since the complete ^1H, ^{15}N, and ^{13}C chemical shift assignments have been made for free 4-OT (Stivers et al., 1996c), and substrates of 4-OT are expected to be in fast exchange on the chemical shift time scale ($k_{off} \sim 10^4$ s^{-1}; Stivers et al., 1996b), it is possible to assign the $^1H-^{15}N$ chemical shifts and determine the dissociation constant of the complex by making successive additions of **4** to an NMR sample containing ^{15}N-labeled 4-OT and monitoring the changes in amide ^1H and ^{15}N chemical shifts in a $^1H-^{15}N$ HSQC spectrum.

The $^1H-^{15}N$ HSQC spectra at 500 MHz of free and **4**-saturated 4-OT are shown in the two panels of Figure 3, and the final ^{15}N and H−N $\Delta\delta$ values ($=\delta_{complex} - \delta_{free}$) are plotted according to residue number in Figure 4A−C. In this titration it was possible to trace the movements of all amide resonances except that of Leu-8, which was observed to disappear at the earliest titration point ([**4**] = 0.32 mM)

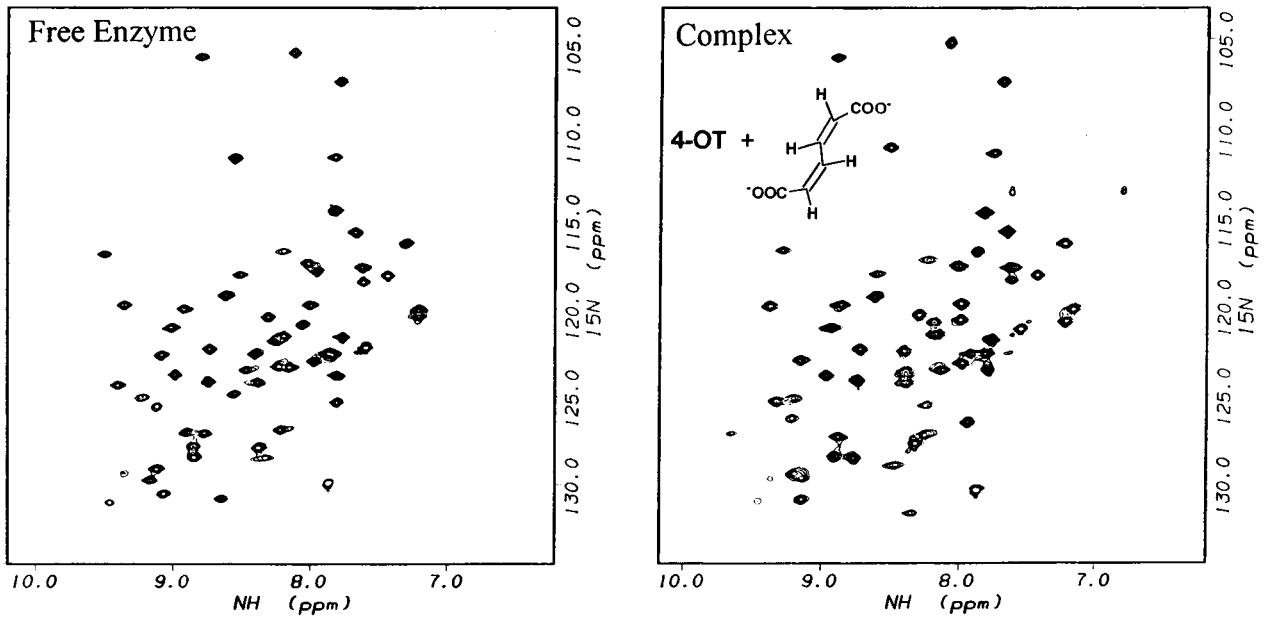

FIGURE 3: $^{1}H-^{15}N$ HSQC spectra of 4-OT (Free Enzyme) and its complex with **4** (Complex) at 500 MHz (pH 6.5, 42 °C). The spectra were recorded with the R_1 pulse sequence ($T = 0$) and acquisition parameters described under Experimental Procedures.

presumably due to exchange broadening. The amide resonance of Leu-8 reappeared at later points in the titration ([**4**] > 6.2 mM) and showed the largest $\Delta\delta$(N−H) of any residue (0.75 ppm, Figure 4B). The amide resonance of Leu-8 was unambiguously assigned on the basis of the following cross peaks seen in a 3D $^{1}H-^{15}N$ NOESY-HSQC spectrum (τ_{mix} = 50 ms): (1) a medium-strength NOE to the H_α of Ile-7, (2) a weak cross-strand NOE between the N−H of Met-45 and the H_α of Leu-8, and (3) a strong NOE between the N−H of Glu-9 and the H_α of Leu-8. In addition, the resonance of Leu-35, which is very weak in the free enzyme due to the combined effects of fast N−H exchange and conformational exchange (Stivers et al., 1996c), is not seen in the complex. Since the amide proton and nitrogen chemical shifts of Leu-35 did not change significantly for the early points in the titration with **4** and the peak heights diminished, it is likely that the chemical shifts for Leu-35 in the free enzyme and complex are similar but that the intensity of Leu-35 in the complex is further weakened such that it is no longer observable above the noise in the spectrum. Thus the $^{15}N-H$ amide cross peaks of all 60 of the non-proline residues of 4-OT were assigned in the free enzyme (Stivers et al., 1996c) and 59 of these 60 were assigned in the complex.

As shown in Figures 4A−C and 2B, the largest chemical shift changes are clustered in active site regions of the enzyme (*i.e.*, Ile-2, loops I and II, and the β-hairpin). Interestingly, Arg-11 and Arg-39, which have been implicated in substrate binding or catalysis (Subramanya et al., 1996; Stivers et al., 1996b,c) both show significant chemical shift changes upon binding **4**. Figure 2B summarizes the regions of the tertiary structure which show changes in ^{15}N and NH chemical shifts upon binding of **4**.

Using eq 1 and the $\Delta\delta$ values for Arg-11, Arg-39, and Gly-51, a $K_D = 0.59 \pm 0.14$ mM for binding of **4** to 4-OT was determined (Figure 4D). No cooperativity in the binding of **4** was observed, consistent with the simple hyperbolic substrate kinetics seen with 4-OT (Whitman et al., 1991). From the end point of the titration, a binding stoichiometry of 1.04 ± 0.06 molecules of **4** per subunit of 4-OT is calculated, consistent with the six active sites per hexamer found using the affinity label 3-bromopyruvate (Stivers et al., 1996a). Hence under the conditions of the NMR experiment 96% of the enzyme is in the binary complex with **4**.

Evidence that **4** binds to the active site of 4-OT was obtained by a kinetic analysis of its inhibition of the isomerization of substrate **2**. The kinetic data indicated linear competitive inhibition by **4** (not shown), with a K_I value of 0.9 ± 0.2 mM as determined from a plot of K_m^{app} against the concentration of **4**. This K_I value overlaps with the K_D value obtained by the NMR titrations.

^{15}N Relaxation Measurements. ^{15}N relaxation data were collected at 42 °C at 500 and 600 MHz field strengths, and representative R_1 and R_2 decay curves (at 600 MHz) for the free enzyme and its complex with **4** are shown in Figure 5, which exemplifies the high quality of the relaxation data. The average standard deviation of the fits for the R_1 and R_2 decay curves were ±4.3% and ±2.4%, respectively, for the free enzyme and ±2.3% and ±2.4%, respectively, for the complex. For one residue, Ser-24, reliable relaxation data were obtained only at 500 MHz, due to resonance overlap with a folded over arginine side chain $N^{\epsilon}H^{\epsilon}$ resonance which prevented accurate measurements using the 600 MHz data set.

R_1 Relaxation. The R_1 values for free 4-OT at 500 and 600 MHz (Figure 6A) are remarkably uniform over most of the molecule, with mean values of 1.15 ± 0.12 and 0.93 ± 0.12 s^{-1} at 500 and 600 MHz, respectively. However, significantly lower values of R_1 are seen in the middle of loop 2 (Ala-33 to Leu-35). Significantly greater than average R_1 values are seen in five regions of the enzyme, β-strand 1 (Ala-3, Gln-4, His-6), the beginning of the α-helix (Asp-13, Glu-14), the end of loop 2 (Ser-37, Arg-39), turn 2 (Gly-48), and the C-terminal coil (Ala-57 to Arg-61). Significant increases in R_1 upon formation of the enzyme−inhibitor complex (Figure 6B) are found in β-strand 1 (Gln-4, Ile-5, Ile-7, Leu-8). Decreases in R_1 occur at the end of the α-helix (Arg-29, Leu-31) and in or near the β-hairpin (His-49, Phe-50, Leu-56, Ala-57). A total of 15 of the 19 residues from

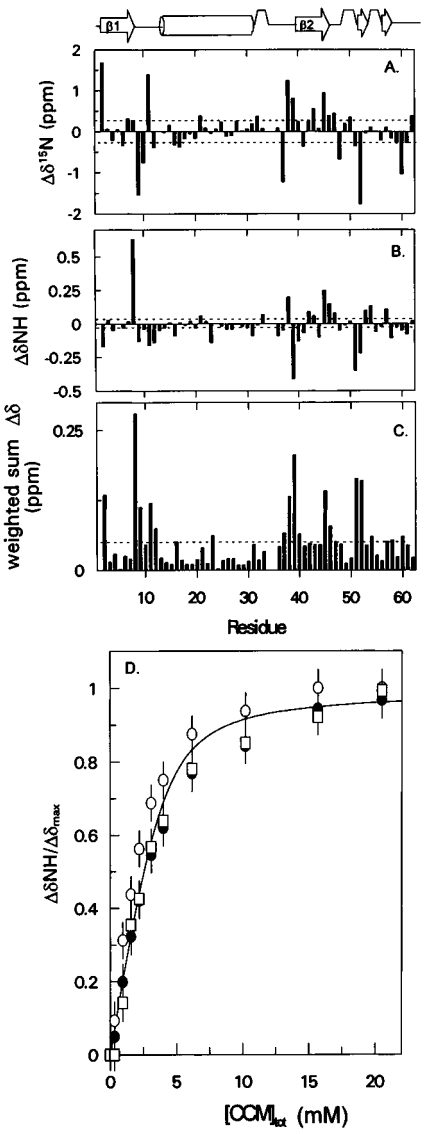

FIGURE 4: Changes in the backbone amide chemical shifts of 4-OT upon binding of **4** and determination of the dissociation constant for the complex. (A) The changes ($\Delta\delta = \delta$[complex] $- \delta$[free enzyme]) in the ^{15}N amide (A) and NH chemical shifts (B) are shown as a function of the amino acid sequence and solution secondary structure of 4-OT. (C) Sum of the absolute magnitude of nitrogen and proton chemical shift changes that were weighted according to the backbone amide chemical shift dispersion in the proton and nitrogen dimensions (2.33 and 27.2 ppm, respectively). Dashed lines in each bar chart indicate the uncertainty threshholds for the $\Delta\delta$ measurements. (D) Determination of the dissociation constant for the complex. The amide proton chemical shifts of Arg-11 (open squares), Arg-39 (closed circles), and Gly-51 (open circles) were followed in a ^{1}H$-^{15}$N HSQC spectrum as the enzyme was titrated with **4** (CCM, *cis*,*cis*-muconate). The curve is the best-fit line through the data using eq 1, with $K_D = 0.59$ mM.

Arg-39 to Ala-57 show decreases in R_1 upon binding of **4**, indicating increased mobility in this region in the complex.

R_2 Relaxation. The R_2 values for free 4-OT (Figure 6C) are uniform over most of the molecule, with mean values of 17.52 and 18.22 s^{-1} at 500 and 600 MHz, respectively. The R_2 values at 600 MHz are consistently greater than the values at 500 MHz. Analysis with the program Modelfree 3.1 (Palmer et al., 1991) in accord with eq 7 shows that many of the backbone amide resonances are broadened by chemical exchange (see below). This exchange contribution (R_{ex}) is not between free enzyme and its complex with **4** because

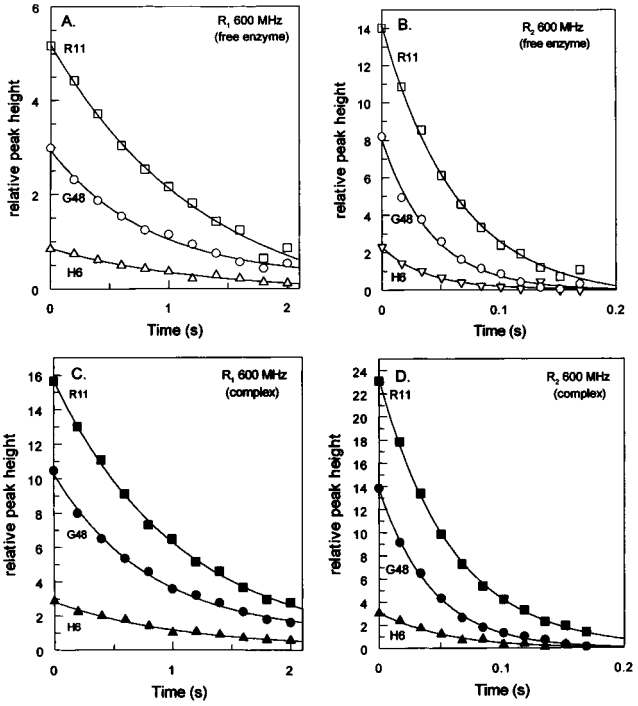

FIGURE 5: Representative R_1 and R_2 decay curves for the free enzyme (panels A and B, respectively) and its complex with **4** (panels C and D, respectively) at 600 MHz. The curves indicate best fits to single exponential decays. Data for residues R11 (squares), G48 (circles), and H6 (triangles) are shown.

96% of the enzyme is in the complexed form (Figure 4D). Residues that have significantly greater R_2 values than the mean are in β-strand 1 (Gln-4, Ile-5, His-6), loop 2 (Leu-35), and turn 2 (Gly-48). R_2 values below the mean occur over the last seven residues, reflecting greater than average mobility.

Upon formation of the complex (Figure 6D), significant increases in R_2 are seen in the β1-strand (Gln-4, Ile-5, Ile-7), loop II (Ser-37, Val-38), the β-hairpin (Ala-57), and the last five residues of the C-terminal coil, reflecting decreased motion in the complex. In contrast, Ser-12 of loop 1 and Asp-32 of turn I show decreases in R_2 values.

$^1H-^{15}N$ NOE Measurements. For a rotational correlation time of 14.2 ns, as has been estimated for 4-OT from an analysis of the R_2/R_1 ratios (see Experimental Procedures), theoretical NOE maxima of 0.81 and 0.83 at 500 and 600 MHz, respectively, are expected. These values are within error of the mean experimental ^{1}H$-^{15}$N steady-state NOE values of 0.79 ± 0.06 and 0.79 ± 0.06 which are calculated from the data at 500 and 600 MHz, respectively, excluding the C-terminal residues 55−62 which have significantly smaller NOEs (Figure 6E), reflecting a greater contribution of high-frequency motion.

NOE measurements are fairly insensitive to the internal dynamics of macromolecules with long correlation times such as 4-OT (Habazettl & Wagner, 1996), and the measurements have relatively low precision compared to the R_1 and R_2 determinations. Hence, the NOE values, except for those of the most mobile regions of the structure, merely confirm the dynamic information provided by the R_1 and R_2 values. Only the C-terminal residues Glu-55 to Arg-62 show NOEs significantly less than the mean values, reflecting greater motion in this region. Significant increases in the NOE values upon formation of the complex are clustered primarily

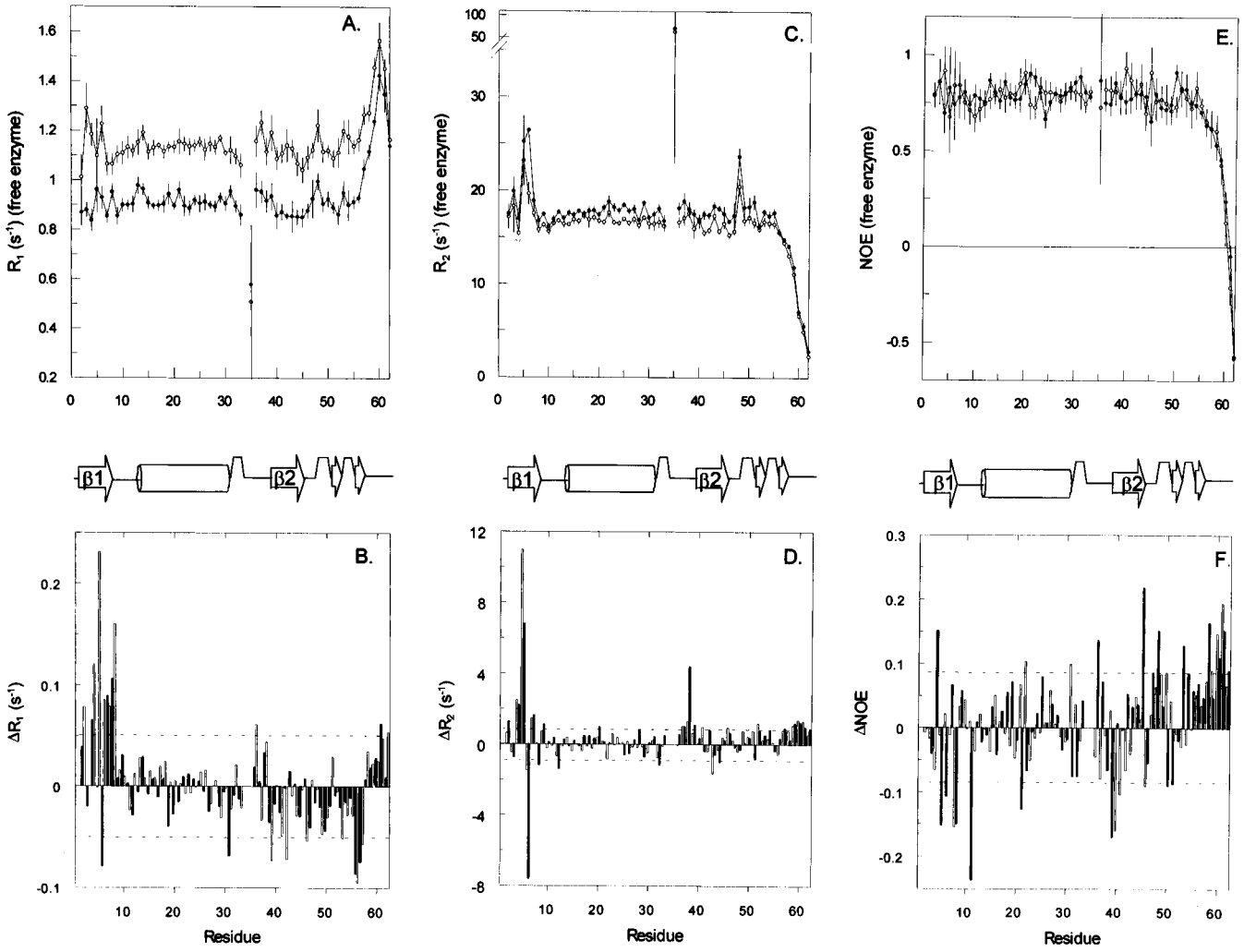

FIGURE 6: Plots of R_1, R_2, and NOE for the free enzyme at 500 and 600 MHz (panels A, C, and E) and the changes in these values upon formation of the complex (panels B, D, and F) as a function of residue number and solution secondary structure. The data acquired at 500 and 600 MHz are shown as open and closed symbols, respectively. For clarity the error bars have been omitted from the Δ plots. Instead, error thresholds are drawn at the mean error for all the measurements. Since many of the individual measurements have errors less than the mean error, some of the $\Delta R_{1,2}$ values below these lines are significant.

in the C-terminal region (Figure 6F), indicating decreased high-frequency motion of this region in the complex.

Model-Free Analysis. The ^{15}N R_1, R_2, and NOE data for each residue were fit simultaneously to the appropriate form of the model-free spectral density function (eq 5 or 6), using the model selection protocol described in detail by Farrow et al. (1994). A term for chemical exchange line broadening (R_{ex}, eq 7) was included when necessary to fit the relaxation data. In the model-free analysis, the overall tumbling of the molecule is assumed to be isotropic and the internal motions are assumed to be independent of the overall tumbling. For 4-OT, this appears to be an excellent assumption since a space-filling model based on the X-ray structure shows that the hexamer is an oblate spheroid with the three principal axes in the ratio of 1.0:0.98:0.71.

An initial estimate of $\tau_m = 14.2 \pm 0.4$ ns for both free 4-OT and the complex was determined from the trimmed weighted mean R_2/R_1 ratios at 500 and 600 MHz (see Experimental Procedures). After assignment of the appropriate spectral density function for each residue, the overall correlation time was then optimized for all residues simultaneously using a grid search for the variable τ_m in addition to optimizing the individual parameters for each residue. The optimized values of τ_m were 13.66 ± 0.08 and 13.73 ± 0.04 ns for the free and complexed enzymes, respectively, which converged from starting points of 9−18 ns.

The model-free spectral density function of Lipari and Szabo (eq 5) was sufficient to model the data for all the residues of the free enzyme except residues Ala-57 to Arg-62, which required the two-time-scale spectral density function (eq 6). The relaxation data for the complex were fit using the same models as the free enzyme except for Leu-56, which required the two-time-scale function only in the complex. In addition, 36 residues of the free enzyme and 47 residues of the complex required an R_{ex} contribution to satisfactorily back-calculate the R_2 relaxation data within their experimental error limits.

Generalized Order Parameters. The mean S^2 value for the entire molecule (excluding Leu-35 and residues 57−62 which have significantly lower values) is 0.87 ± 0.03, indicating that the nanosecond to picosecond motion of most of the backbone NH vectors of 4-OT is highly restricted (Figure 7A). Residues showing significantly greater mobility than the mean ($0.5 \leq S^2 \leq 0.83$) are found in the active site regions of loop 1 (Glu-9), loop 2 (Leu-35), the β-hairpin (Leu-56, Ala-57), and β-strands 1 and 2 (Ile-2, Glu-44, Met-45), as well as in C-terminal residues 58−62 ($0.03 \leq S^2 \leq 0.70$). Residues showing lesser mobility than the mean (S^2

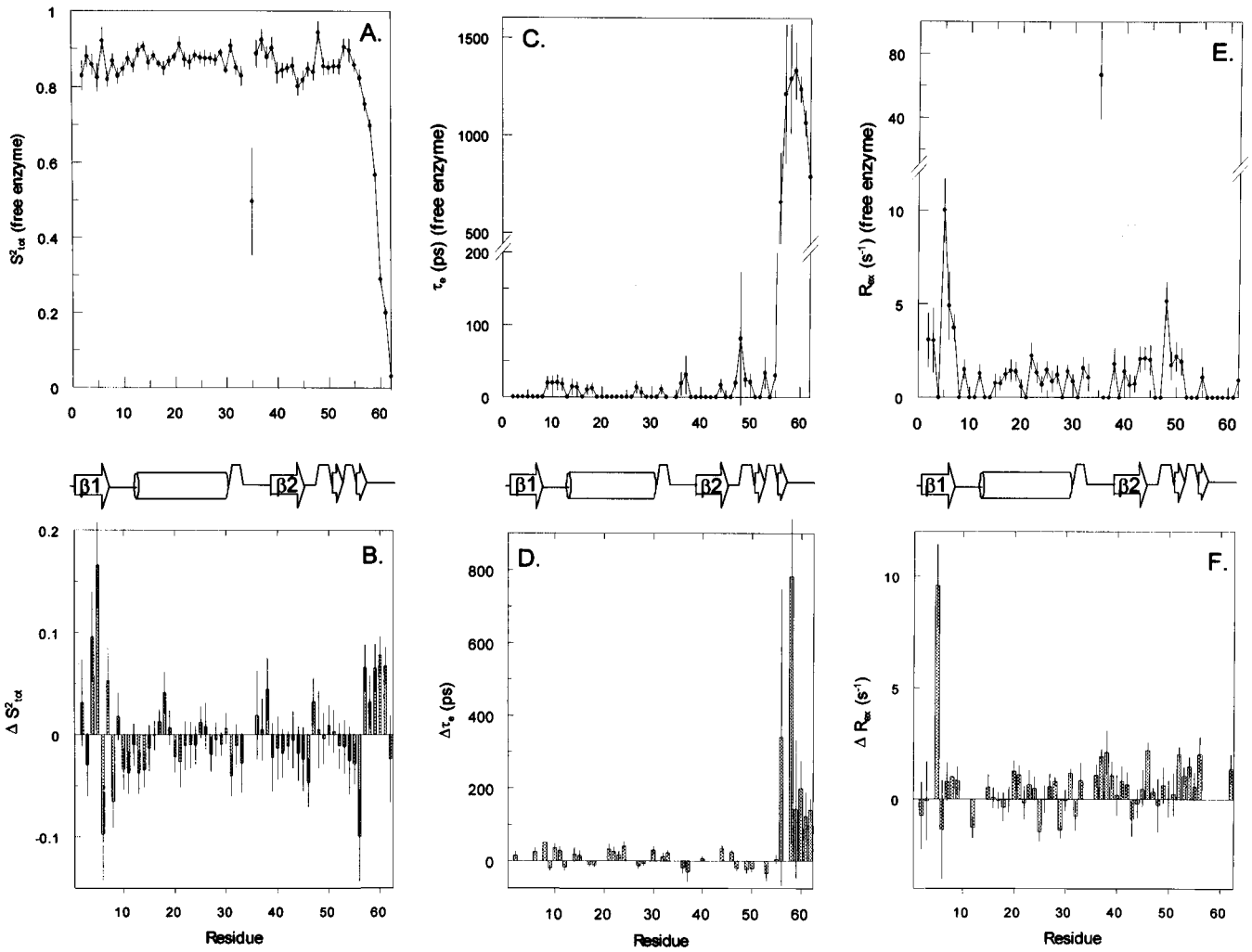

FIGURE 7: Plots of the order parameters (S^2), internal correlation times (τ_e), and R_{ex} values for the free enzyme (panels A, C, and E) and the changes in these parameters upon formation of the complex (panels B, D, and F) as a function of residue number and solution secondary structure. For residues L56 to R62, the order parameter $S^2 = S^2_s S^2_f$ (see eq 6).

≥ 0.90) are seen in the β1-strand (Ile-5, His-6), loop 2 (Ser-37), and turn 2 (Gly-48).

Many of the changes in S^2 upon binding of **4** (Figures 2C and 7B) were localized to residues at or near the active site. Significant increases in S^2, reflecting more restricted motion in the complex, are seen in loop 2 (Val-38) and the β-hairpin (Ala-57). Significant decreases in S^2, reflecting less restricted internal motion in the complex, are seen in the β1-strand (Leu-8), loop 1 (Gly-10), the α-helix (Asp-13, Glu-14), Ala-46, and the β-hairpin (Leu-56). Increases in S^2 outside of the active site, induced by the binding of **4**, are seen in the β1-strand (Gln-4, Ile-5), the α-helix (Thr-18), and the C-terminal coil (residues 58−61). Decreases in S^2 induced by the binding of **4** are seen in the β1-strand (His-6) and turn 1 (Leu-31).

The τ_e values for internal motions faster than the overall correlation time were small for most residues of the free enzyme and the complex, although larger τ_e values were required for seven residues in the C-terminal coil (Figure 7C). For free 4-OT, the τ_e term in eq 5 was not required to model the relaxation data for 32 residues, as a result of S^2 values >0.87 and/or τ_e values <10 ps. Values of τ_e between 10 and 80 ps were required for 19 residues. Residues Leu-56 to Arg-62 of the C-terminal coil required large τ_e values, falling in the range ∼700−1400 ps, together with low order parameters as noted above. For the complex, a τ_e term was not required for 34 residues, again due to large S^2 values and/or very low τ_e values, and τ_e values between 6 and 55 ps were required for 18 residues. The largest increases in τ_e on complex formation were in the C-terminal residues Ser-58 and Val-60 to Arg-62, suggesting that the complex has slower motions in this region (Figure 7D).

Chemical Exchange Parameter (R_{ex}). Thirty-seven of the 60 observable resonances of the free enzyme required an R_{ex} term (Figure 7E). The largest R_{ex} contributions to the line width were seen in the β1-strand (Ile-5, His-6, Ile-7), loop 2 (Leu-35), and turn 2 (Gly-48). Significant increases in R_{ex} on binding of **4** occurred at the active site in loop 2 (Thr-36 to Val-38), Arg-39, and turn 2 (Lys-47) and in four residues of the β-hairpin (Ile-52, Gly-53, Gly-54, Leu-56) (Figures 7F and 2D). Overall, 47 residues in the complex required an R_{ex} term with 16 residues requiring a larger value than the free enzyme and 3 residues requiring a smaller value.

DISCUSSION

*Chemical Shift Changes upon Binding of **4**.* The residues that show the largest changes in ^{15}N and H−N chemical shifts when **4** binds are localized in three-dimensional space to regions surrounding the active site (Figure 2A,B). In fact, most of the changes are clustered around residues that have been assigned a role in catalysis (Pro-1, Phe-50) or substrate

Table 1: Effect of Binding of **4** on Backbone NH Entropy[a]

immobilized residue	$S^2_{complex}$	S^2_{free}	$-T\Delta\mathbf{S}$ (kcal/mol)	mobilized residue	$S^2_{complex}$	S^2_{free}	$-T\Delta\mathbf{S}$ (kcal/mol)
Q4	0.96 ± 0.03	0.86 ± 0.03	0.72	H6	0.82 ± 0.03	0.92 ± 0.04	−0.51
I5	0.99 ± 0.02	0.82 ± 0.04	1.80	L8	0.80 ± 0.02	0.87 ± 0.02	−0.25
T18	0.89 ± 0.01	0.85 ± 0.02	0.20	G10	0.81 ± 0.01	0.85 ± 0.02	−0.13
A57	0.82 ± 0.01	0.75 ± 0.02	0.20	D13	0.86 ± 0.01	0.90 ± 0.02	−0.19
K59	0.63 ± 0.02	0.57 ± 0.01	0.10	E14	0.87 ± 0.01	0.91 ± 0.01	−0.22
V60	0.37 ± 0.01	0.29 ± 0.02	0.08	L31	0.87 ± 0.01	0.91 ± 0.02	−0.22
R61	0.27 ± 0.01	0.20 ± 0.02	0.06	A46	0.80 ± 0.01	0.85 ± 0.02	−0.17
				L56	0.72 ± 0.04	0.82 ± 0.02	−0.28
			sum: 3.2 ± 1.1[b]				sum: -1.9 ± 0.1

[a] $-T\Delta\mathbf{S}$ contributions to ΔG were calculated with the equation $\Delta G = -T\Delta\mathbf{S} = -RT \ln[(1 - S^2_{complex})/(1 - S^2_{free})]$ (Akke et al., 1993). [b] This large standard deviation results from the large error of ±1.0 kcal/mol for $-T\Delta\mathbf{S}$ of I5.

binding (Arg-11, Arg-39) (Stivers et al., 1996a,b; Subramanya et al., 1996). The clustered changes in chemical shifts for active site loops 1 and 2, and the β-hairpin, show that these regions change chemical environment upon binding of the substrate analog, due either to conformational changes in the enzyme or to electronic effects of **4** on the amide chemical shifts.

The chemical shift changes for both Arg-11 and Arg-39 upon binding of **4** provide evidence in support of the suggestion, based on the crystal structure of free 4-OT, that Arg-39 and Arg-11, respectively, interact with the 1- and 6-carboxylate groups of **1** (Subramanya et al., 1996). The observation that the backbone NH chemical shifts of *both* Arg-11 and Arg-39 change when the dicarboxylic acid **4** binds (while the side chain and backbone resonances of Arg-29 and Arg-21 do not) is significant because covalent binding of the monocarboxylic acid substrate analog 3-bromopyruvate altered the chemical shifts of Arg-39 only (Stivers et al., 1996c). Taken together, these results indicate that the 1- and 6-carboxylate groups of the substrate interact with Arg-39 and Arg-11, respectively. From the crystal structure (Figure 2A) this interaction would be with Arg-39 from one subunit and with Arg-11′ from an adjacent subunit (Subramanya et al., 1996). The precise orientation of the substrate in the active site is an important question because Arg-11 and Arg-39 are also candidates for the putative general acid catalyst (AH, Figure 1). These results make Arg-39 a much stronger candidate. Other candidates are His-49 and Lys-47 (Stivers et al., 1996c).

The amide proton resonance of Leu-8, which is ~4 Å from the nitrogen atom of Pro-1, the catalytic base, is profoundly deshielded upon formation of the complex ($\Delta\delta = 0.75$ ppm downfield). In fact, Leu-8, the last residue of the β1-strand, has the most downfield-shifted amide proton resonance (9.63 ppm) in the complexed enzyme. This large deshielding effect suggests that this proton is more strongly hydrogen bonded in the complex or that the edge of the π-electron cloud of **4** is deshielding this NH proton.

Solution Dynamics of Free and Complexed 4-OT. In relating the backbone and side chain dynamics of 4-OT to its mechanism of action, we note that events important to catalysis such as substrate binding (4×10^6 M^{-1} s^{-1}), enzyme turnover ($k_{cat} = 1100$ s^{-1}), and product release (≥ 1100 s^{-1}) occur at rates in the microsecond to millisecond time scale of motions which affect R_{ex}. Other events, such as fluctuations in the positions of enzyme groups, or intramolecular proton transfers, may occur in the subnanosecond time scale, detected by the order parameter S^2 and correlation time τ_e for high-frequency motions.

With respect to high-frequency motions, assuming that changes in S^2 result solely from changes in amplitude of such motions, seven residues, including one active site residue, Ala-57, show increased restriction of backbone motion upon binding of **4** (Table 1). Decreased restriction of backbone motion is found in eight residues including six active site residues (Figures 7B and 2C, Table 1). Thus no uniform freezing or immobilization of the backbone has occurred in the active site when **4** binds. The absence of large increases in the backbone order parameters for active site regions of 4-OT is not unexpected because these regions (loop 1, loop 2, and the β-hairpin) already have high order parameters in the free enzyme, with the exception of Leu-35 (Figure 7A). The only region of the enzyme that shows a uniform increase in the order parameter (and in τ_e) upon binding of **4** is the C-terminal coil, the most mobile region in the free enzyme.

Some of the largest changes in S^2 upon binding of **4** occur in the β1-strand, which shows a loose pattern of alternating increases and decreases in S^2 (Figures 7B and 2C). Interestingly, those amide groups involved in *intersubunit* hydrogen bonds show increased mobility on ligand binding (His-6, Leu-8), while amide groups involved in *intrasubunit* hydrogen bonds show decreased mobility (Ile-5).[2] Thus the binding of the substrate analog appears to have loosened quaternary (intersubunit) interactions and tightened tertiary (intrasubunit) interactions. These quaternary effects are consistent with the substrate analog interacting with both Arg-39 and Arg-11′ on adjacent subunits (Figure 2A) and may also be responsible for the observed negative cooperativity in the covalent inactivation of 4-OT by the substrate-based affinity label, 3-bromopyruvate (Stivers et al., 1996a).

Several studies have examined the effects of ligand binding on protein *backbone* dynamics, and diverse effects have been reported. In a study of the effects of calcium binding on the backbone dynamics of calbindin (Akke et al., 1993), a large increase in the average S^2 value for a loop region involved directly in metal binding was seen. In contrast, a study of the effects of phosphotyrosine−peptide binding on the backbone dynamics of the SH2 domain (Farrow et al., 1994) found only a single residue in the peptide binding site which showed a large increase in S^2 upon complex forma-

[2] Alternating patterns of high and low S^2 values have been reported in a β-strand of free *E. coli* ribonuclease H (Mandel et al., 1995) and in a β-strand of the p53 tetramer (Clubb et al., 1995) depending on whether the NH vector was hydrogen bonded to an adjacent strand or was exposed to solvent. The 4-OT−inhibitor complex provides the first example of such an alternation at a subunit interface as a result of ligand binding.

tion, while other binding site residues showed decreases or no effect. From these phosphopeptide binding results it was concluded that for the backbone there was no "simple relationship between peptide binding and large-scale restriction of picosecond time scale dynamics in the binding site" (Farrow et al., 1994).

With respect to side chain dynamics, increases in S^2 upon ligand binding have generally been found. In studies on the effect of nucleotide and Ca^{2+} binding to staphylococcal nuclease (Nicholson et al., 1992), and steroid binding to the enzyme Δ^5-3-ketosteroid isomerase (Zhao et al., 1996), it was concluded that ligand binding induced a localized restriction of motion in side chains around the ligand binding site. In a study of the effects of phosphotyrosine−peptide binding on the methyl group dynamics of the SH2 domain, restriction of motion upon peptide binding was found for residues that interacted with the phosphotyrosine subsite, while methyl groups that interacted with hydrophobic regions of the bound phosphotyrosine−peptide showed the opposite effect or no effect (Kay et al., 1996).

In each of the above studies, when a significant increase in the order parameter was observed for a residue in the ligand binding site, the S^2 values for the free proteins were in the range ~0.6−0.75, values which are much lower than the average order parameter for the active site regions of free 4-OT ($\langle S^2_{\text{free}} \rangle = 0.85$). Thus, on the basis of the above observations we conclude that ligand binding produces diverse effects on backbone and side chain dynamics. The presence of large-amplitude, high-frequency motions in the free state, and the "freezing out" of these motions when a ligand binds, while often observed, is not a universal principle governing ligand−macromolecule interactions.

It is of interest to ask whether the changes in the S^2 values for the backbone NH vectors of 4-OT upon binding of **4** are energetically significant. As described by Akke et al. (1993), it is possible, using experimentally measured order parameters, to estimate the entropic contributions of fast time scale motions to the Gibbs free energy of binding with eq 8. In

$$\Delta G = G_{\text{complex}} - G_{\text{free}} = -RT\sum_{j=1}^{N}\ln[(1 - S^2_{j,\text{complex}})/(1 - S^2_{j,\text{free}})] \quad (8)$$

this equation, ΔG is the difference in free energy between the complexed and free enzyme resulting only from changes in high-frequency motions of the NH vectors, $S^2_{j,\text{complex}}$ and $S^2_{j,\text{free}}$, respectively, are the order parameters for a given NH vector in the bound and free enzyme, and the sum is taken over the N vectors. This analysis assumes that the motions of the NH vectors are not correlated and that changes in S^2 result solely from changes in amplitude of their high-frequency motion. Of the 59 S^2 values measured for the backbone NH vectors in both the free and liganded enzymes, seven showed significant increases and another eight showed significant decreases in S^2 on ligand binding (Figures 2C and 7B, Table 1). Using eq 8, we calculate that the seven residues which showed increases in S^2 yield a total entropic ($-T\Delta\mathbf{S}$) contribution to $\Delta G_{\text{binding}}$ of $+3.2 \pm 1.1$ kcal/mol, while the eight residues with decreases in S^2 yield a total $\Delta G_{\text{binding}}$ of -1.9 ± 0.1 kcal/mol (Table 1). The net positive ΔG of $+1.3 \pm 1.1$ kcal/mol suggests a partial entropic compensation for the freezing of some backbone motions on ligand binding by the mobilization of others. If the compensating increases in mobility did not occur, the overall free energy change for binding of **4** to the enzyme would be less favorable, by at least 1.9 kcal/mol, on the basis of this analysis of high-frequency backbone motions only. This unfavorable free energy change associated with the restriction of high-frequency motions of some backbone NH vectors upon the binding of **4** is significant compared to the overall free energy of binding of **4**, which is −4.6 kcal/mol as calculated from the K_D value of 0.59 mM. Thus, these results suggest that enzymes may diminish the entropic penalty associated with "freezing" the motions of backbone or side chain groups upon substrate binding by increasing the high-frequency motions of other regions of the molecule.

Low-Frequency Motions (Millisecond to Microsecond) in Free and Bound 4-OT. In addition to the order parameter S^2 which measures the restriction of picosecond to nanosecond motions, it is of interest to examine the slower time scale processes which are detected by the R_{ex} contribution to the line width and compare these values in the free and ligand-bound enzyme. A rigorous interpretation of R_{ex} is complicated because this parameter is a function of not only the rate constant for exchange but also the chemical shift difference and fractional populations at the exchanging sites (Epstein et al., 1995, and references therein). Therefore, we can only suggest that the R_{ex} term reflects the existence of a dynamic exchange process in the microsecond to millisecond time scale.

A number of residues in the β1-strand show significant R_{ex} terms which may reflect a subtle sliding or breathing motion of this strand in both the free enzyme and the complex (Figure 7E,F). Whatever the detailed nature of this motion, it is important to point out that all of the residues in the β1-strand have high order parameters and extremely slow NH exchange rates ($t_{1/2} \gg 64$ h) and are therefore not exposed to solvent by any conformational exchange process that may be occurring. Leu-35 of the free enzyme also shows a large exchange contribution to its line width. However, in contrast to residues in the β1-strand, Leu-35 is highly mobile ($S^2 = 0.5 \pm 0.15$) and is in rapid exchange with solvent. Since the residues surrounding Leu-35 have high order parameters and low R_{ex} values, it appears that the high- and low-frequency motions of Leu-35 are highly localized. A possible explanation for this unique behavior is that Leu-35 is located in the middle of a loop and is preceded by a proline residue, which may serve to rigidify the backbone and isolate the local motions of Leu-35.

In contrast to the high-frequency backbone motions monitored by the order parameter S^2, there is a more uniform correlation between active site regions and an increase in R_{ex} upon binding of the substrate analog (Figures 7F and 2D). These exchange contributions are not between free enzyme and its complex with **4** because 96% of the enzyme is in the complexed form (Figure 4D). Furthermore, there is no simple correlation between the magnitudes of the ligand-induced ^{15}N chemical shift changes and the ΔR_{ex} values (Figures 4A and 7F). In the active site, three residues of loop 2 (Thr-36, Ser-37, Val-38) as well as Arg-39, which interacts with the 1-carboxyl group of **4**, show an increase in R_{ex}. In addition, residues Ile-52 through Glu-55 of the β-hairpin show increased R_{ex} values in the complex, while Asp-13 in loop 1 is the only active site residue which shows a decrease in R_{ex} (Figures 2D and 7F). Thus, active site

residues show backbone motions in the microsecond to millisecond time scale in both the free enzyme and the substrate analog complex which may be required for substrate binding, product release, and catalysis.

SUPPORTING INFORMATION AVAILABLE

Two tables (S1 and S2) containing the experimental R_1, R_2, and NOE values and two tables (S3 and S4) containing the calculated values of S^2, τ_e, and R_{ex} for both free and complexed 4-OT (12 pages). Ordering information is given on any current masthead page.

REFERENCES

Abeygunawardana, C., Stivers, J. T., Whitman, C. P., & Mildvan, A. S. (1996) Experimental NMR Conference, Asilomar, CA, March 17−22, Abstract MP74.

Abragam, A. (1961) *The Principles of Nuclear Magnetism*, Clarendon Press, Oxford.

Akke, M., Skelton, N. J., Palmer, A. G., III, & Chazin, W. J. (1993) *Biochemistry 32*, 9832−9844.

Cheng J.-W., Lepre, C. A., & Moore, J. M. (1994) *Biochemistry 33*, 4093−4100.

Clore, G. M., Driscoll, P. C., Wingfield, P. T., & Gronenborn, A. M. (1990a) *Biochemistry 29*, 7387−7401.

Clore, G. M., Szabo, A., Bax, A., Kay, L. E., Driscoll, P. C., & Gronenborn, A. M. (1990b) *J. Am. Chem. Soc. 112*, 4989−4991.

Clubb, R. T., Omichinski, J. G., Sakaguchi, K., Appella, E., Gronenborn, A. M., & Clore, G. M. (1995) *Protein Sci. 4*, 855−862.

Epstein, D. M., Benkovic, S. J., & Wright, P. E. (1995) *Biochemistry 34*, 11037−11048.

Farrow, N. A., Muhandiram, R., Singer, A. U., Pascal, S. M., Kay, C. M., Gish, G., Shoelson, S. E., Pawson, T., Forman-Kay, J. D., & Kay, L. E. (1994) *Biochemistry 33*, 5984−6003.

Habazettl, J., & Wagner, G. (1996) *J. Magn. Reson. 109*, 100−109.

Hiyama, Y., Niu, C.-H., Silverton, J. V., Bavoso, A., & Torchia, D. A. (1988) *J. Am. Chem. Soc. 110*, 2378−2383.

Jencks, W. P. (1987) *Cold Spring Harbor Symp. Quant. Biol. 7*, 65−73.

Kay, L. E., Torchia, D. A., & Bax, A. (1989) *Biochemistry 28*, 8972−8979.

Kay, L. E., Muhandiram, D. R., Farrow, N. A., Aubin, Y., & Forman-Kay, J. D. (1996) *Biochemistry 35*, 361−368.

Leatherbarrow, R. J. (1992) *Grafit*, Version 3.0, Erithacus Software Ltd., Staines, U.K.

Levy, G. C., & Lichter, R. L. (1979) *Nitrogen-15 NMR Spectroscopy*, John Wiley and Sons Inc., New York.

Lipari, G., & Szabo, A. (1982a) *J. Am. Chem. Soc. 104*, 4546−4559.

Lipari, G., & Szabo, A. (1982b) *J. Am. Chem. Soc. 104*, 4559−4570.

Mandel, A. M., Akke, M., & Palmer, A. G., III (1995) *J. Mol. Biol. 246*, 144−163.

Mildvan, A. S. (1974) *Annu. Rev. Biochem. 43*, 357−399.

Mori, S., Abeygunawardana, C., Johnson, M. O., & van Zijl, P. C. M. (1995) *J. Magn. Reson. 108B*, 94−98.

Nicholson, L. K., Kay, L. E., Baldisseri, D. M., Arango, J., Young, P. E., Bax, A., & Torchia, D. A. (1992) *Biochemistry 31*, 5253−5263.

Palmer, A. G., III, Rance, M., & Wright, P. E. (1991) *J. Am. Chem. Soc. 113*, 4371−4380.

Pandell, A. J. (1976) *J. Org. Chem. 41*, 3992−3996.

Peng, J. W., & Wagner, G. (1994) *Methods Enzymol. 239*, 563−596.

Press, W. H., Flannery, B. P., Teukolsky, S. A., & Vetterling, W. T. (1992) *Numerical Recipes in Fortran*, 2nd ed., Cambridge University Press, Cambridge.

Rischel, C., Madsen, J. C., Andersen, K. V., & Poulsen, F. M. (1994) *Biochemistry 33*, 13997−14002.

Sklenar, V., Torchia, D., & Bax, A. (1987) *J. Magn. Reson. 73*, 375−379.

Stivers, J. T., Abeygunawardana, C., Mildvan, A. S., Hajipour, G., Whitman, C. P., & Chen, L. H. (1996a) *Biochemistry 35*, 803−813.

Stivers, J. T., Abeygunawardana, C., Mildvan, A. S., Hajipour, G., & Whitman, C. P. (1996b) *Biochemistry 35*, 814−823.

Stivers, J. T., Abeygunawardana, C., Whitman, C. P., & Mildvan, A. S. (1996c) *Protein Sci. 5*, 729−741.

Stone, M. J., Fairbrother, W. J., Palmer, A. G., Reizer, J., Saier, M. H., & Wright, P. E. (1992) *Biochemistry 31*, 4394−4406.

Stone, M. J., Chandrasekhar, K., Holmgren, A., Wright, P. E., & Dyson, H. J. (1993) *Biochemistry 32*, 426−435.

Subramanya, H. S., Roper, D. I., Dauter, Z., Dodson, E. J., Davies, G. J., Wilson, K. S., & Wigley, D. B. (1996) *Biochemistry 35*, 792−802.

Whitman, C. P., Aird, B. A., Gillespie, W. R., & Stolowich, N. J. (1991) *J. Am. Chem. Soc. 113*, 3154−3162.

Whitman, C. P., Hajipour, G., Watson, R. J., Johnson, W. H., Jr., Bembenek, M. E., & Stolowich, N. J. (1992) *J. Am. Chem. Soc. 114*, 10104−10110.

Zhao, Q., Abeygunawardana, C., & Mildvan, A. S. (1996) *Biochemistry 35*, 1525−1532.

BI961834Q